J. Phys.: Condens. Matter **11** (1999) 9483–9494. Printed in the UK PII: S0953-8984(99)05985-8

Magnetic quantum wells

F J Himpsel

Department of Physics, University of Wisconsin Madison, 1150 University Avenue, Madison, WI 53706-1390, USA

E-mail: himpsel@comb.physics.wisc.edu

Received 13 July 1999, in final form 9 September 1999

Abstract. Magnetic properties of materials can be tailored in nanostructures, such as thin films, wires and dots. This article gives an overview of what is known about the electronic states that are relevant for magnetic phenomena, such as oscillatory coupling, giant magnetoresistance (GMR) and spin-polarized tunnelling. These states are probed by high-resolution photoemission and inverse photoemission. Methods for fabricating one- and zero-dimensional structures are explored, such as stripe and dot arrays obtained by step decoration.

1. Motivation

Electronic properties of semiconductor devices have been controlled by introducing heterostructures, quantum wells and superlattices. Magnetism as a cooperative phenomenon lends itself to manipulation in small structures [1], where neighbour atoms can be replaced systematically by species with stronger or weaker magnetism. In fact, a class of magnetic/nonmagnetic multilayers termed 'spin valves' has recently been introduced by IBM into commercial reading heads for magnetically stored data.

A simple, particle-in-a-box model tells us that the spectrum of electronic states is going to change when electrons are confined to dimensions comparable to their wavelength (figure 1). The smooth, three-dimensional density of states breaks up into a train of singularities in one dimension. These are caused by quantum well states. Their positions can be manipulated by adjusting the width of the confining potential. Thereby, a high density of states can be placed at the Fermi level E_F, which may trigger electronic phase transitions, such as magnetism, superconductivity or charge density waves. The well known Stoner criterion for spontaneous formation of ferromagnetic order involves the overall density of states at the Fermi level. Likewise, antiferromagnetism can be traced to high density of states at particular momenta k that match the q-vector of the antiferromagnetic order. More recently, it has become clear that oscillations in the magnetic coupling of multilayers are generated by density-of-states oscillations at the Fermi level induced by quantum well states [2–5].

Conductivity and magnetoresistance are also determined by electrons at the Fermi level. In order to contribute to charge and spin transport, electrons have to lie within a thermal energy kT of the Fermi level ($kT = 25$ meV at room temperature). Recent progress in high-resolution photoelectron spectroscopy has made this energy regime accessible [6, 7]. Such measurements are k-resolved, making it possible to pick out the relevant k-states that dominate the k-integrated transport data. Currently, there is great interest in spin currents. Generating and controlling them is the main topic of the emerging field of magnetoelectronics [8].

0953-8984/99/489483+12$30.00

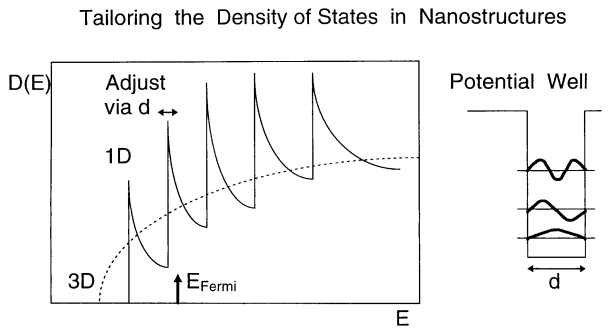

Figure 1. Tailoring of electronic states in nanostructures. Confinement creates quantum well states that enhance the density of states $D(E)$ at specific energies. High density of states at the Fermi level E_F affects electronic transport properties and triggers electronic phase transitions, such as magnetism, superconductivity and charge density waves.

When attempting to produce tailored magnetic materials one might ask the question how fine a structure needs to be in order to have an impact on the electronic and magnetic properties. As an estimate we may use the Fermi wavelength λ_F of a simple free electron gas. It decreases with increasing carrier density. Therefore, confinement and quantization phenomena are visible in semiconductors already at dimensions achievable by standard lithography, whereas in metallic magnets such phenomena do not appear until one reaches dimensions of a few nanometres. Actually, the Fermi wavelength of typical metals has atomic dimensions, but beat frequencies with the lattice can produce an envelope function with a much larger wavelength (for example $\lambda_{env} = 2$ nm in Cu(100) films [1–3]). Therefore, structures in the single digit nanometre regime are expected to produce the maximum impact.

Going from the traditional thin-film structures towards lower-dimensional objects, such as wires and dots, one would expect an ever larger effect of the confinement. The end of this article will give an outlook on the various methods that are being tested for producing magnetic nanowires and dots by self-assembly. A particular focus will lie on nanostructures with linear order, such as arrays of stripes and strings of dots. They lend themselves to the linear readout methods that have dominated the magnetic storage industry, e.g. the use of reading heads in tapes and disks. There is a variety of self-assembly methods to choose from. Here we focus onto concepts that utilize a stepped surface as template [9]. Adsorbed atoms, molecules or clusters have a tendency to stick to the step edges where they find extra bonding partners for lateral bonds. Ideally, one hopes to decorate the step edges with magnetic stripes or strings of magnetic particles. The current status and an outlook onto promising avenues will be provided.

2. Spin-dependent reflectivity and confinement

Can quantum well states modify the electronic and magnetic structure of a material, as suggested in figure 1? In fact, the oscillatory magnetic coupling observed in magnetic layer structures can be traced to magnetic quantum well states [2, 5]. Figure 2 shows that a significant modulation of the density of states at the Fermi level can be achieved in the vicinity of specific k-points [3]. The simple picture of an electron interferometer works quite well here. The Fe/Co and Cu/vacuum interfaces act as electron mirrors that induce standing waves in the Cu film [1, 10]. When the thickness of the Cu film is increased one observes interference maxima every half wavelength, as in a Fabry–Pérot interferometer. The relatively long wavelength

$\lambda = 2$ nm obtained from these data is not the (much shorter) Fermi wavelength of Cu, but that of the envelope function of the quantum well state. In reciprocal space, the corresponding wavevector $k_{env} = 2\pi/\lambda$ represents the small difference between two large wavevectors, i.e. the Fermi wavevector k_F and the Brillouin zone boundary $k_{BZ} = \pi/d_{100}$, which is determined by the lattice spacing in the [100] direction. In real space this may be viewed as a beat frequency between the Fermi wavelength and the atom spacing. The oscillating density of states from states at the Fermi level is sampled by atoms residing at discrete lattice spacings.

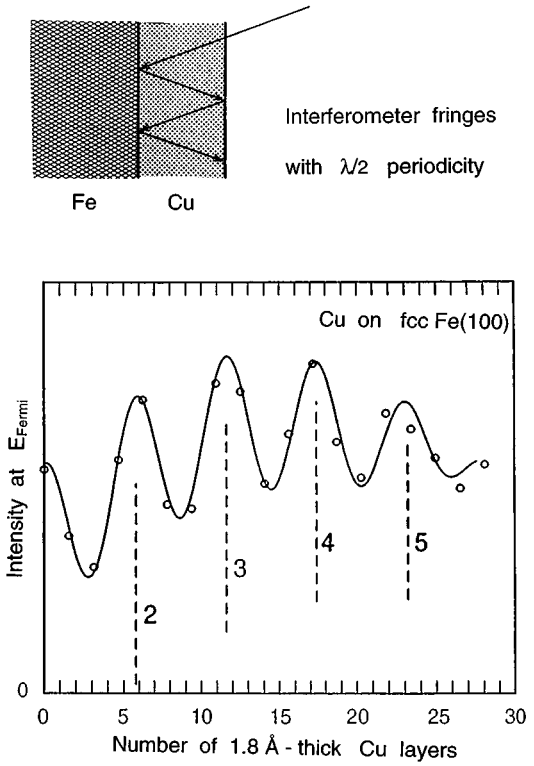

Figure 2. Oscillations in the density of states $D(E)$ with film thickness caused by quantum well states in a Cu film on fcc Fe(100). A simple interferometer model explains the oscillations as interference fringes and shows that such an experiment directly measures the wavelength of the (envelope) wavefunction. After Ortega *et al* [3].

In a magnetic coupling experiment the vacuum interface is replaced by a second magnetic layer on top of the Cu layer, e.g. a Co layer or a magnetically softer permalloy layer in actual disk reading heads. It is found that the magnetic coupling between the two layers oscillates when the thickness of the Cu layer is increased. The period is identical to that of the quantum well state oscillations in figure 2. Such an agreement has been found wherever comparable data exist, e.g. for Ag/bcc Fe(100), Au/bcc Fe(100), Cu/fcc Co(100), Cu/fcc Fe(100), Cr/bcc Fe(100). Actually, a single combination of materials can have several periodicities, which correspond to quantum well states located in different regions of k-space. For example, the well studied Co/Cu/Co(100) system exhibits an additional, shorter oscillation period ($\lambda = 0.5$ nm) which originates from states at the neck of the Cu Fermi surface, as opposed to the states from the belly that give rise to the oscillations in figure 2. The two periods are shown in figure 3 and compared to oscillations in the magnetic coupling [4].

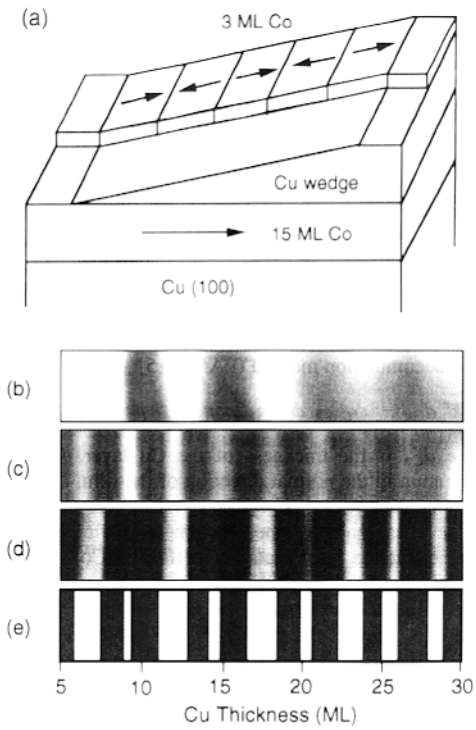

Figure 3. Long and short period oscillations in the magnetic coupling for Co/Cu/Co(100) and the corresponding oscillations in the density of states at two k-points. (a) Schematic drawing of the wedge sample. (b) Photoemission density of states of the long-period quantum well states at the belly of the Fermi surface. (c) Photoemission density of states of the short-period quantum well states at the neck of the Fermi surface. (d) Oscillatory magnetic coupling between the two Co layers from magnetic linear dichroism. (e) Fit of the oscillatory coupling to the two quantum well state oscillations. From Kawakami *et al* [4].

Quantum well states by themselves cannot affect magnetic coupling unless they are spin polarized. It is somewhat puzzling at first to postulate that quantum well states in a non-magnetic Cu layer carry spin information. Experimentally one finds that they do [7, 11, 12]. Figure 4 shows spin-polarized photoemission data of the short-period quantum well states [7] in Cu/Co(100) which suggest a set of discrete quantum well states with minority spin on top of the majority spin continuum. The explanation for the spin polarization of quantum well states is based on a spin-dependent electron reflectivity of the interfaces, an effect that also plays a role in giant magnetoresistance as well. Using again the simple interferometer picture, one has to take into account that the reflectivity at a ferromagnetic interface differs between majority and minority spins. The magnetic exchange splitting splits the bands in the ferromagnet and produces a spin-dependent barrier of the inner potential. For majority spins, the barrier is small since the majority d bands of Co are filled, i.e. noble-metal-like. The minority spin bands of Co lie higher than those in Cu and produce an energy barrier that confines them to the Cu layer. The situation is expected to be reversed for spacer layers to the left of the ferromagnets in the periodic table, such as Cr. One would expect quantum well states with majority spin character. Quantum well states have been observed in Cr [13] but their spin polarization has not yet been measured.

A quantitative connection between quantum well states and magnetic coupling can be made by calculating the total energy of all occupied states and minimizing it between the

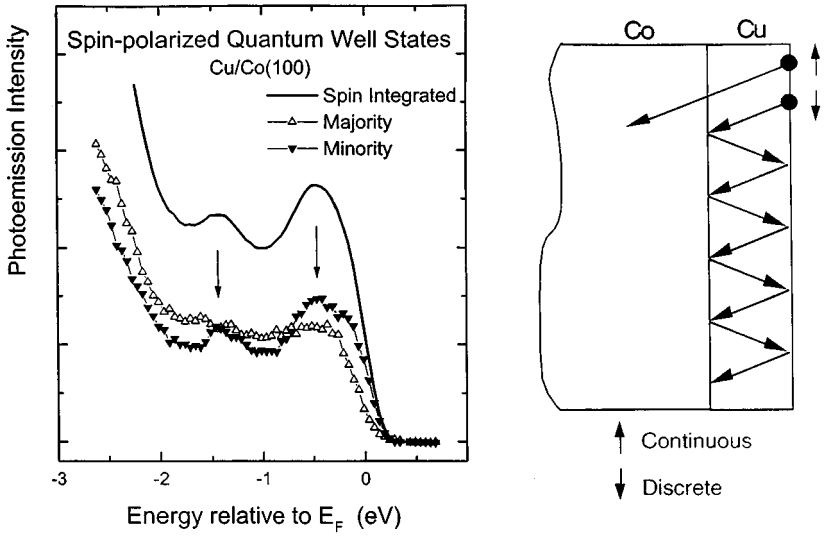

Figure 4. Spin-polarized photoemission of short-period quantum well states in Cu/Co(100) demonstrating their minority spin character. The spin-dependent electron reflectivity of the interface with Co explains how spin polarization can be induced in a non-magnetic metal, such as Cu. After Ortega *et al* [7].

two magnetic configurations, parallel and antiparallel [2, 5]. Magnetic quantum well states are supported by the parallel configuration only. In the antiparallel configuration, one of the interfaces reflects electrons of a given spin and the other transmits them. Consequently, the total energy is a continuous function of the thickness in the antiparallel configuration but drops discontinuously whenever a quantum well state moves above the Fermi level and becomes unoccupied. The resulting change in the energy balance drives the magnetic switching. This quantum well picture of magnetic coupling can be mapped mathematically onto the traditional RKKY picture of magnetic coupling through an electron gas. It turns out that the main features of the two models, such as the oscillation periods, agree in most cases. Only quantitative results differ, such as the coupling strength. That is due to the fact that the RKKY model originates from lowest order perturbation theory, whereas the quantum well state model does not make any assumptions about the strength of the interaction.

On the experimental side, it has been difficult to observe quantum well states in magnetic multilayers until better preparation methods for smooth interfaces were found. This is particularly true for the short wavelength states. That becomes clear from the optical interferometer analogue [10], which requires the roughness of a mirror to be small compared to the wavelength. Special deposition techniques had to be developed for reproducibly obtaining short period quantum well states [4, 7, 12]. They involve deposition at low temperature for preventing island nucleation and interface diffusion. Subsequent annealing to room temperature restore full crystallinity. The substrates need to be ultra-smooth as well, which can be achieved by careful electropolishing or the use of whiskers with highly perfect surfaces [13, 14].

3. Consequences for magnetoelectronics

Spin-polarized electron reflectivity at magnetic interfaces creates not only quantum well states, but also influences other phenomena that are utilized in magnetoelectronics, such as giant

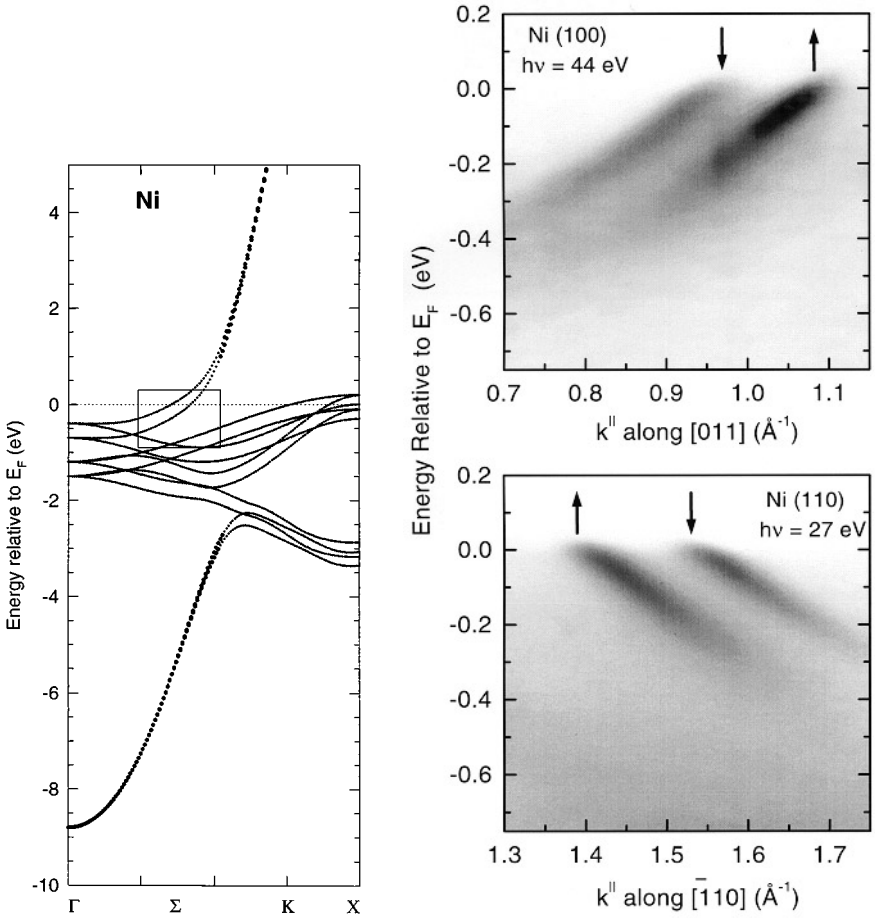

Figure 5. $E(k)$ band dispersions of Ni along the [110] direction showing flat d bands and a steep, parabolic s,p band. The states relevant for charge and spin transport in magnetoelectronics are located at the Fermi level crossing where the s,p band starts hybridizing with the uppermost d band (box). High-resolution photoemission with angular multidetection is able to resolve the spin-split band crossing the Fermi level. Two data sets from the (100) and (110) surfaces map out the boxed-in area of the band structure in opposite directions. From Himpsel *et al* [7].

magnetoresistance (GMR) [15]. Generally, the GMR effect is more complex than magnetic coupling, but it is based on spin-dependent scattering, either in the bulk or at interfaces. The fundamental unit in GMR structures is the same as that in magnetic coupling, i.e. a pair of ferromagnetic layers separated by a non-magnetic spacer. The ferromagnetic layers and their interfaces act as spin filters for electrons, based on the different scattering probabilities in the bulk and at the interface: for parallel magnetization of the two ferromagnets we have parallel spin filters with a high transmission; for antiparallel magnetization the spin filters are opposite to each other and block the current. An external magnetic field switches the configuration from antiparallel to parallel, thereby reducing the resistance.

While GMR is based on spin-dependent scattering in the bulk as well as at the interfaces, there is a fair amount of evidence that the interfaces dominate. Experiments with multilayers of the same overall thickness but different number of periods suggest that there is a strong

interface component to the GMR effect. Interface scattering also causes the GMR to be larger in the CPP geometry (conductivity perpendicular to the plane) than in CIP (conductivity in plane) where electrons can bypass the interfaces. Therefore, a stronger reflection of minority spins than majority spins at the interface will not only create spin-polarized quantum well states but also contribute to GMR. The question remains whether the spin-dependent interface scattering in GMR is mainly specular, as for quantum well states, or diffuse.

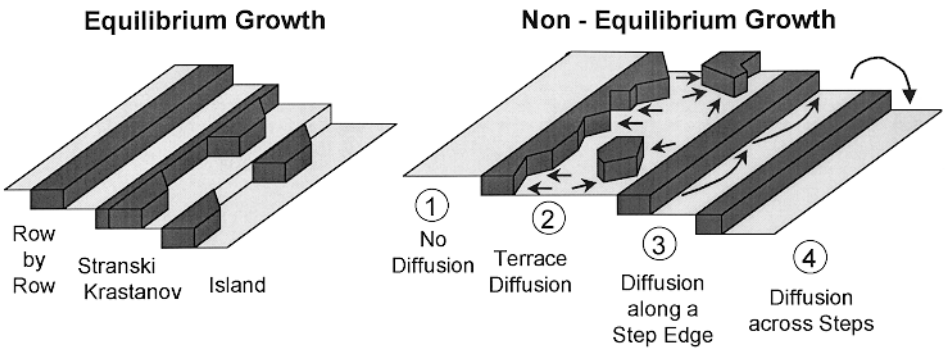

Figure 6. Growth modes observed at stepped surfaces. In addition to the usual equilibrium growth modes one observes at least four non-equilibrium modes for Cu on stepped Mo(110). They are characterized by thermal activation of diffusion along the terraces, along the step edges and across the steps. Compare Himpsel *et al* [9].

Another promising phenomenon in magnetoelectronics is spin-polarized tunnelling [16, 17]. It gives rise to a magnetoresistance effect analogous to that in GMR, except that the spacer layer is insulating instead of metallic. The corresponding electrical properties are different (e.g. lower power consumption), which makes tunnel junctions interesting as non-volatile memory elements rather than sensors. Spin-dependent tunnelling occurs between various combinations of ferromagnets, normal metals and superconductors, all separated by a thin insulating barrier (typically 1–2 nm Al_2O_3). Since the tunnelling probability decays exponentially by factor of $\approx 10^2$ for a single atom diameter it is clear that the interface and magnetic transport across nanometre-sized layers will play a major role. The effective barrier quickly increases for electrons tunnelling at energies below E_F, letting only electrons within a few tenths of an eV below E_F participate in tunnelling. Of those, the s,p electrons with their more delocalized wavefunctions leak out the farthest and are expected to dominate the tunnelling matrix element. In fact, the spin polarization of d states at the Fermi level would give the wrong sign for the spin polarization in Ni and Co. Since the majority d band is full in Ni and Co the minority d states dominate at the Fermi level. A simple free electron model for the s,p electrons explains the majority spin polarization seen in tunnelling from ferromagnets into superconductors [16]. Integrating a constant density of states in three-dimensional $\boldsymbol{k}$-space over the Fermi sphere $|\boldsymbol{k}| \leqslant k_F$ one obtains a total s,p-electron density $N \sim k_F^3 \sim E_F^{3/2}$ and a density of states $n = \mathrm{d}N/\mathrm{d}E \sim E_F^{1/2} \sim k_F$. The corresponding spin polarization at E_F is [16]:

$$P_{Free} = [(n_\uparrow - n_\downarrow)/(n_\uparrow + n_\downarrow)] = [(k_{F\uparrow} - k_{F\downarrow})/(k_{F\uparrow} + k_{F\downarrow})].$$

That fits the data for Fe quite well ($P_{Tunnel} = 40\%$ versus $P_{free} = 43\%$ [16]) and it did fit early results for Ni. However, the experimental spin polarization in Ni has increased substantially as better tunnel junctions became available and is now incompatible with the free electron model

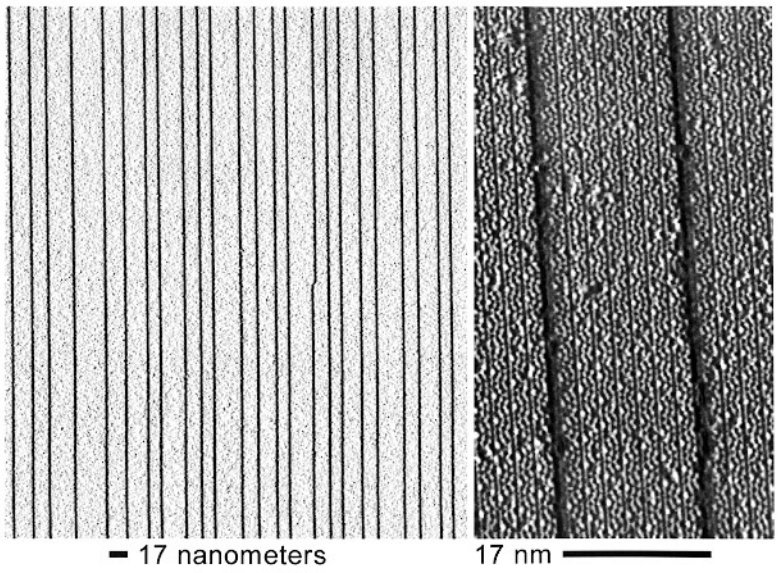

Figure 7. Preparation of straight steps on Si(111)7 × 7. The overview on the left shows only a single kink in 20 000 edge atoms (340 × 390 nm^2). The close-up on the right (40 × 70 nm^2) shows atomically straight step edges following the natural grooves in the 7 × 7 surface that separate areas of opposite stacking. The derivative of the STM topography is shown, giving the appearance of a surface being illuminated from the left. After Viernow *et al* [28].

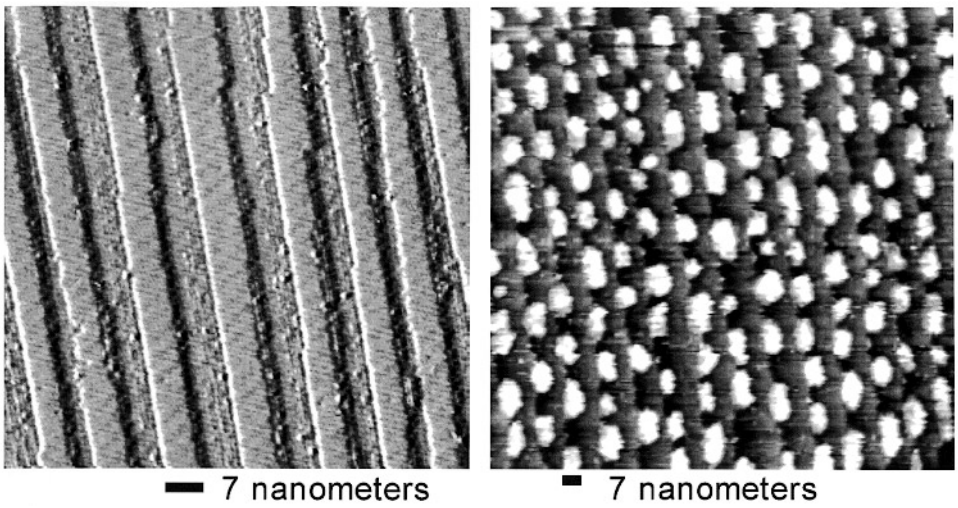

Figure 8. Arrays of CaF_2 stripes and dots, lined up along steps of a Si(111)7 × 7 surface. The dot density is 3×10^{11} cm^{-2}, or 2 Teradots/in^2. From Viernow *et al* [29].

($P_{Tunnel} = 23$–33% versus $P_{free} = 6\%$ when using de Haas–van Alphen and photoemission data for for k_F).

This discrepancy in Ni calls for a more refined model. First one should take the actual Fermi surface with its $\boldsymbol{k}$-dependent magnetic splitting into account, instead of using a free-electron Fermi surface with a constant splitting. In addition to the correct Fermi surface one

has to take the actual spin polarization at E_F into account [6, 7]. It can be observed indirectly in high-resolution photoemission experiments by resolving the two spin components at E_F and determining their area ratios (see figure 5, right side). From the Ni(100) data (top) one obtains an area ratio $A_\uparrow/A_\downarrow = 1.8$. That gives a spin polarization of 29% at this particular $\boldsymbol{k}$-point in a particular geometry. The data from Ni(110) at the bottom give a lower ratio of $A_\uparrow/A_\downarrow = 1.2$, resulting in a spin polarization of 9%. This polarization of 9%–29% is to be compounded with the 6% spin polarization expected from the different size of the majority and minority spin Fermi surface. The resulting total polarization comes closer to the 23–33% observed in tunnelling [16, 17], particularly when considering a depolarization at higher temperature. (Our results are for 200 K, whereas the tunnelling data were taken at much lower temperatures.) Current work is directed towards a systematic mapping of the spin polarization for different locations on the Fermi surface of the s,p band and an assessment of the spin-dependent photoemission matrix element [18]. Current theories of spin-polarized tunnelling are considering the analogous tunnelling matrix element [19].

The data in figure 5 give an example of the qualitative progress that has been made in angle-resolved photoemission in recent years. The energy resolution has reached a level of 10 meV and better which lies well below the thermal energy, even at temperatures below room temperature. That makes the states within kT of the Fermi level accessible that are responsible for charge and spin transport, which form the basis of magnetoelectronics. Angular multidetection, such as in figure 5, improves the k-resolution to a level where it becomes smaller than the k-broadening $\delta k = 1/l_e$ induced by the finite scattering length l_e of the electrons at the Fermi level. That makes it possible to measure the spin-dependent mean free path. For example, a 20% admixture of Fe to Ni in permalloy reduces the minority spin mean free path by almost an order of magnitude down to 0.6 nm [6] whereas the majority spin mean free path remains large at about 4 nm. Such a spin anisotropy contributes to the bulk part of the GMR effect. Currently, the states are being sought that cause this strong spin dependence [20]. Other alloying materials, such as Cr, are expected to affect the majority spins more than the minority spins and thus provide the complete arsenal for controlling spin transport.

4. One- and zero-dimensional structures

After demonstrating the idea of tailoring electronic states for two-dimensional layer structures it is natural to proceed towards lower dimensions where the density of states is expected to be affected even more by confinement. Instead of the steplike density of states at the edge of a two-dimensional sub-band, one obtains a $1/\sqrt{E}$ singularity and a δ-function, respectively. Getting down to the single-digit nanometre level by conventional writing or lithography techniques is difficult and slow. For producing macroscopic amounts of such materials it would be desirable to find self-assembly techniques. A variety of methods are currently being tested (for the fabrication of wire structures see [9, 21–30]). Here we give a progress report on an effort to utilize stepped Si surfaces [28] as templates for producing linear arrays of stripes and dots [29, 30]. The idea is to develop a 'universal' fabrication method that allows the deposition of arbitrary materials (ferromagnets, noble metals, insulators) onto a substrate of choice, such as Si, borrowing as many techniques from Si microlithography as possible. The first step consists of preparing highly perfect step arrays on silicon, the second of decorating these steps with a mask material by self-assembly and the third step of selective etching or deposition, for example by selective adsorption, chemical vapour deposition or electroplating.

The first step has been highly successful (figure 7): on the Si(111)7 $\times$ 7 surface it has been possible to create steps with only a single kink in 20 000 edge atoms by a straightforward annealing sequence [28]. As mask material, epitaxial CaF_2 has been tested [29]. Depending

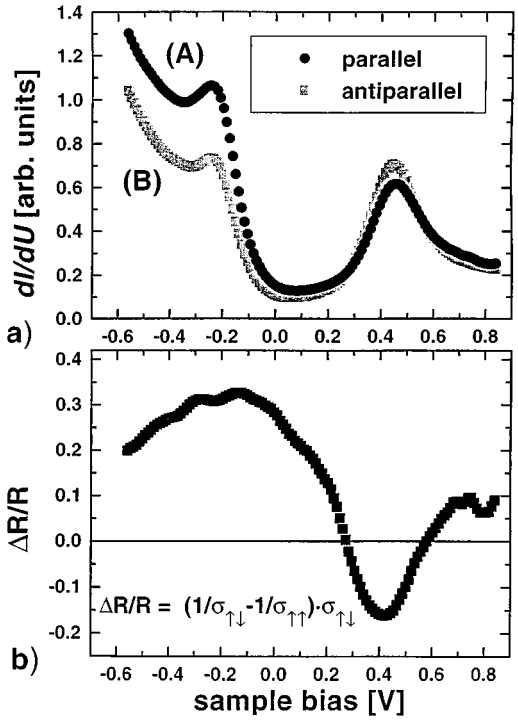

Figure 9. Spin-polarized scanning tunnelling spectroscopy of a magnetically split surface state at the Gd(0001) surface. By scanning a magnetic Gd surface with a magnetic Fe tip one obtains tunnelling spectra that depend on the relative orientation of the magnetic moments of tip and sample (a). That leads to a magnetoresistance when switching the magnetic orientation of the Gd surface (b). From Wiesendanger *et al* [34].

on the coverage and growth temperature, CaF_2 grows in stripes or forms strings of nano-dots attached to the Si step edges (figure 8). These are typically 7 nm wide and 15 nm apart. Dot arrays with densities of 2 Teradots per square inch have been produced which might become useful as masks for patterned magnetic storage media. The stripe spacing can be controlled by the miscut angle of the Si wafer, the stripe width by the CaF_2 coverage. Selective deposition of organic molecules has been demonstrated on CaF_2 stripe arrays [30], including nickelocene, a promising precursor for depositing carbon- and oxygen-free Ni by photolysis. With silicon templates there are many other options for borrowing deposition and etching techniques from silicon technology. Eventually, one could consider incorporating nanostructures into Si-based microdevices on the same chip.

The electronic structure of such one- and zero-dimensional systems and their magnetic behaviour are just beginning to be explored. Scanning probe techniques become essential for probing electronic states and magnetism on the nanometre scale [31]. Scanning tunnelling spectroscopy, in particular, looks rather promising for detecting quantized states in such structures. Such states have been observed already in non-magnetic systems, such as in two-dimensional Pb films on Si(111)7 $\times$ 7 [32] and on one-dimensional terraces [33]. The spin-polarized version of scanning tunnelling spectroscopy [31] has made a breakthrough recently [34–36] and appears on track for becoming a probe of magnetism in nanometre-size structures that are below the resolution limit of current techniques, such as magnetic force microscopy

(MFM). An example is shown in figure 9 [34]. A magnetized Fe tip is used to tunnel either into an empty minority spin surface state or out of an occupied majority spin surface state of Gd(0001). The Fe tip emits and accepts predominantly electrons polarized parallel to its magnetization and thus enhances tunnelling from the majority spin surface state when tip and sample have parallel magnetization (A). Tunnelling into the unoccupied minority-spin surface states becomes stronger after switching the magnetically softer Gd with an external field (B). In this anti-parallel configuration the unoccupied state is polarized parallel to the tip. Magnetic surface states have been observed on other surfaces as well, such as Fe(100) and Cr(100) [37], suggesting that this method is applicable to a wider class of systems. Even in the absence of a specific surface state one expects a magnetoresistance effect in scanning tunnelling spectroscopy similar to that for spin-polarized tunnelling across planar Al_2O_3 junctions.

Acknowledgment

This work was supported by the NSF under award Nos DMR-9815416 and DMR-9704196. It was partly conducted at the SRC, which is supported by the NSF under award No DMR-9531009.

References

[1] For an overview of magnetic nanostructures see Himpsel F J, Ortega J E, Mankey G J and Willis R F 1998 *Adv. Phys.* **47** 511
[2] Edwards D M, Mathon J, Muniz R B and Phan M S 1991 *Phys. Rev. Lett.* **67** 493
[3] Himpsel F J 1991 *Phys. Rev.* B **44** 5966
Ortega J E and Himpsel F J 1992 *Phys. Rev. Lett.* **69** 844
Ortega J E, Himpsel F J, Mankey G J and Willis R F 1993 *Phys. Rev.* B **47** 1540
[4] Kawakami R K, Rotenberg E, Escorcia-Aparicio E J, Choi H J, Wolfe J H, Smith N V and Qiu Z Q 1999 *Phys. Rev. Lett.* **82** 4098
[5] Stiles M D 1993 *Phys. Rev.* B **48** 7238
Koelling D D 1994 *Phys. Rev.* B **50** 273
Bruno P 1995 *Phys. Rev.* B **52** 411
Bruno P *J. Phys.: Condens. Matter* at press
[6] Petrovykh D Y, Altmann K N, Höchst H, Laubscher M, Maat S, Mankey G J and Himpsel F J 1998 *Appl. Phys. Lett.* **73** 3459
[7] Himpsel F J, Altmann K N, Mankey G J, Ortega J E and Petrovykh D Y 1999 *J. Magn. Magn. Mater.* **200** 456
Ortega J E, Närmann A, Altmann K N, O'Brien W, Seo D J, Himpsel F J, Segovia P, Mascaraque A and Michel E G 1999 *J. Magn. Magn. Mater.* **203** 126
[8] Prinz G A 1999 *J. Magn. Magn. Mater.* **200** 57
[9] For an overview of step decoration see Himpsel F J, Jung T, Kirakosian A, Lin J-L, Petrovykh D Y, Rauscher H and Viernow J 1999 *MRS Bull.* **24** (8) 20
[10] Bader S D 1999 *Nature* **398** 105
Himpsel F J 1999 *Science* **283** 1655
[11] Garrison K, Chang Y and Johnson P D 1993 *Phys. Rev. Lett.* **71** 2801
Carbone C, Vescovo E, Rader O, Gudat W and Eberhardt W 1993 *Phys. Rev. Lett.* **71** 2805
[12] Kläsges R, Schmitz D, Carbone C, Eberhardt W, Lang P, Zeller R and Dederichs P H 1998 *Phys. Rev.* B **57** R696
[13] Dongqi Li, Pearson J, Bader S D, Vescovo E, Huang D-J, Johnson P D and Heinrich B 1997 *Phys. Rev. Lett.* **78** 1154
[14] Paggel J J, Miller T and Chiang T-C 1999 *Science* **283** 1709
[15] Parkin S S P *J. Phys.: Condens. Matter* at press
[16] Meservey R and Tedrow P M 1994 *Phys. Rep.* **238** 173
[17] Moodera J S, Nowak J and van de Veerdonk R J M 1998 *Phys. Rev. Lett.* **80** 2941
[18] Altmann K N, Petrovykh D Y, Mankey G J, Shannon N, Gilman N, Hochstrasser M, Willis R F and Himpsel F J to be published
[19] Slonczewski J C 1989 *Phys. Rev.* B **39** 6995

Mathon J 1997 *Phys. Rev.* B **56** 11 810
MacLaren J M, Zhang X-D and Butler W H 1997 *Phys. Rev.* B **56** 11 827
[20] Franco N *et al* to be published
[21] Piraux L, George J M, Despres J F, Leroy C, Ferain E, Legras R, Ounadjela K and Fert A 1994 *Appl. Phys. Lett.* **65** 2484
Blondel A, Meier J P, Doudin B and Ansermet J-Ph 1994 *Appl. Phys. Lett.* **65** 3019
Liu K, Nagodawithana K, Searson P C and Chien C L 1995 *Phys. Rev.* B **51** 7381
[22] Himpsel F J, Mo Y W, Jung T, Ortega J E, Mankey G J and Willis R F 1994 *Superlatt. Microstruct.* **15** 237
Jung T, Schlittler R, Gimzewski J K and Himpsel F J 1995 *Appl. Phys.* A **61** 467
[23] Paunov M and Bauer E 1987 *Appl. Phys.* A **44** 201
Mundschau M, Bauer E and Swiech W 1989 *J. Appl. Phys.* **65** 581
[24] Mo Y W and Himpsel F J 1994 *Phys. Rev.* B **50** 7868
Jung T, Mo Y W and Himpsel F J 1995 *Phys. Rev. Lett.* **74** 1641
[25] de la Figuera J, Huerta-Garnica M A, Prieto J E, Ocal C and Miranda R 1995 *Appl. Phys. Lett.* **66** 1006
Shen J, Skomski R, Klaua M, Jenniches H, Sundar Manoharan S and Kirschner J 1997 *Phys. Rev.* B **56** 2340
[26] Elmers H J, Hauschild J, Höche H, Gradmann U, Bethge H, Heuer D and Köhler U 1994 *Phys. Rev. Lett.* **73** 898
Hauschild J, Elmers H J and Gradmann U 1998 *Phys. Rev.* B **57** R677
[27] Petrovykh D Y, Himpsel F J and Jung T 1998 *Surf. Sci.* **407** 189
[28] Viernow J, Lin J-L, Petrovykh D Y, Leibsle F M, Men F K and Himpsel F J 1998 *Appl. Phys. Lett.* **72** 948
Lin J-L, Petrovykh D Y, Viernow J, Men F K, Seo D J and Himpsel F J 1998 *J. Appl. Phys.* **84** 255
[29] Viernow J, Petrovykh D Y, Men F K, Kirakosian A, Lin J-L and Himpsel F J 1999 *Appl. Phys. Lett.* **74** 2125
[30] Rauscher H, Jung T A, Lin J-L, Kirakosian A, Himpsel F J, Rohr U and Mullen K 1999 *Chem. Phys. Lett.* **303** 363
Lin J-L, Rauscher H, Kirakosian A, Himpsel F J and Dowben P A, *J. Appl. Phys.* at press **86**
[31] Wiesendanger R 1998 *Scanning Probe Microscopy* ed R Wiesendanger (Berlin: Springer) ch 4 p 71
[32] Altfeder I B, Matveev K A and Chen D M 1997 *Phys. Rev. Lett.* **78** 2815
[33] Avouris Ph and Lyo I-W 1994 *Science* **264** 942
[34] Bode M, Getzlaff M and Wiesendanger R 1998 *Phys. Rev. Lett.* **81** 4256
Wiesendanger R, Bode M and Getzlaff M, to be published
[35] Wulfhekel W and Kirschner J 1999 *Proc. STM'99* ed Y Kuk, I W Lyo, D Jeon and S-I Park p 222
[36] Kim T-H, Choi Y-J, Park W-G, Obukhov Y and Kuk Y 1999 *Proc. STM'99* ed Y Kuk, I W Lyo, D Jeon and S-I Park p 224
[37] Davies A, Stroscio J A, Pierce D T and Celotta R J 1996 *Phys. Rev. Lett.* **76** 4175